Design of minimal synthetic circuits with sensory feedback for quadruped locomotion

Matteo Lodi*, Andrey Shilnikov†, Marco Storace*
*DITEN, University of Genoa, Via Opera Pia 11a, I-16145 Genova, Italy
E-mail: matteo.lodi@edu.unige.it, marco.storace@unige.it
†Neuroscience Institute, and Department of Mathematics & Statistics, Georgia State University
100 Piedmont Ave, Atlanta GA 30303, USA, E-mail: ashilnikov@gsu.edu

***Abstract*—This paper discusses practical approaches for designing reduced synthetic circuits of central pattern generators (CPGs) for quadruped locomotion using our newly developed bifurcation toolkit. Specifically, two CPGs containing only four elements (cells) are proposed that can reliably generate natural gaits of typical quadrupeds more effectively than large dedicated complex networks do. In addition, we analyze an enhanced locomotion system that incorporates a neuromechanical model for each leg and includes mechanisms of sensory feedback. We demonstrate how the proposed CPGs produce the desired gaits, which remain robust with respect to external perturbations.**

I. Introduction

Locomotion in vertebrates with (four) legs is produced by the coordinated limb movements, which, in turn, are determined by frequency, duty-cycle and phase of the rhythmic pattern controlling each limb. The coordination is provided by specific neuron networks, called central pattern generators (CPGs). A CPG can generate single or multiple rhythmic motor activities without sensory feedback, external and/or pacing inputs [1]. A multifunctional CPG is a neural circuit designed to produce different rhythmic outcomes depending on an input coming from the brainstem, which is, in turn, under the control of basal ganglia and cortex functions [2]. The rhythm produced by a CPG is meant to be robust to small perturbations and well maintainable and adaptive via mechanisms of sensory feedback. In other terms, in addition to the open-loop control provided by the CPG, the locomotion system has local (in each limb) closed-loop circuits producing reflexes triggered by environmental interaction. This is one of the reasons why the locomotion system of vertebrates ensures both robustness and variety.

A CPG in a complex vertebrate can be composed of hundreds of neurons grouped in subsets that often behave coherently, i.e., in synchrony. Activity in each functional module, henceforth called a *cell*, can be represented uniformly and thus modeled individually. This allows for a drastic functional reduction of repetitive dynamics from a large CPG network to a smaller circuit containing a few cells only. Of course, the level of abstraction of a CPG model can be very different: networks coming from biological studies often contain too many cells to be suitable for analysis based on tools within the framework of dynamical systems theory. There have been many recent efforts of reductions of large networks to their simplified cores, while preserving some of their pivotal properties and providing plausible explanations for experimental observations [3].

In this paper we propose and discuss practical approaches for designing reduced synthetic circuits of CPGs for quadruped locomotion using our newly developed bifurcation toolkit [4], based on the toolbox CEPAGE [5]. In addition, we test the robustness of these CPGs by adding a neuromechanical model of each leg, and by introducing a direct sensory feedback to verify whether the CPG can properly reset the gait after the occurrence of temporary mechanical perturbations, which can be an external force holding and accelerating either leg for some time as in the case of stumbling. Our results prove the robustness of the CPG rhythmic outcomes.

II. 4-cell CPGs for quadrupedal locomotion

In [4] we introduced a bio-inspired 8-cell CPG, which was derived from a quadrupedal 40-cell CPG [6]. Its rhythmic capacity was analyzed to show that it can reliably generate various gaits typical of most quadrupeds. The 8-cell CPG, shown in Fig. 1(a), has four cells to drive extensor (E) muscles and four to drive flexor (F) muscles. The temporal characteristics of gaits – such as the frequency, duty cycle and phase lags between four legs – are controlled by a parameter (henceforth denoted as α) representing some input descending from the brainstem. The basic idea to further simplify the 8-cell CPG is to remove the extensor cells and their connections: flexor muscles are still driven by the flexor cells, whereas extensor muscles are activated when flexor cells are silent. Properties of cells – such as dynamical model, synapses and the brainstem input – remain the same as in the original 8-cell CPG, see [4] for details. Before introducing the reduced 4-cell CPGs, let us first analyze the behavior of the 8-cell CPG when all its extensor cells are removed. In what follows we will refer to this circuit as the CPG-0 (shown in Fig. 1(b)), which will be below analyzed and compared with the 8-cell CPG to understand the role played by the extensor cells.

A. *CPG-0 circuit*

One can see from Fig. 2 that removing the extensor cells from the 8-cell CPG alters only slightly the duty cycle and the frequency of the flexor cells. Furthermore, we found that the extensors play a fundamental role in determining the quadruped gaits with exact phase lags in the patterns controlling the limbs [4], [7]–[9]. The bifurcation diagram in Fig. 3 demonstrates how the phase-locked phase lags (i.e., their steady-state values), $\Delta\phi_{1i}$, between the reference cell 1 (see the cell number within each colored circle) and other cells change as the parameter α is increased. The diagram reveals that the CPG-0, like the 8-cell CPG, can also stably generate trot ($0.14 < \alpha < 0.78$) and bound gaits ($\alpha > 0.8$), but does

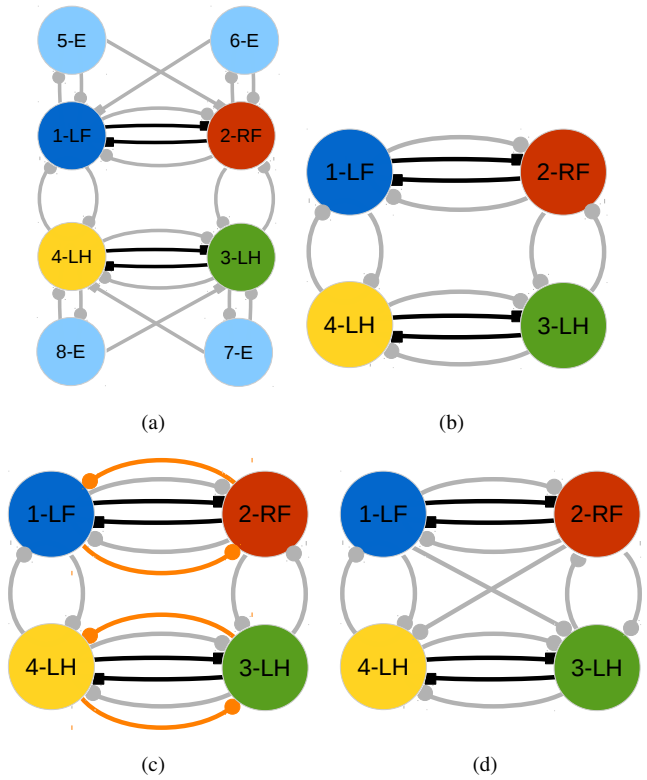

Fig. 1. Circuitries of the 8-cell CPG (a), CPG-0 (b), CPG-A (c) and CPG-B (d). Gray (black) connections represent inhibitory (excitatory) chemical synapses, whereas orange connections represent delayed inhibitory synapses. In the 4-cell CPGs, the cells drive flexor muscles in each leg (L=left, R=right, F=fore, H=hind), whereas the extensor muscles are activated when the corresponding cells are silent.

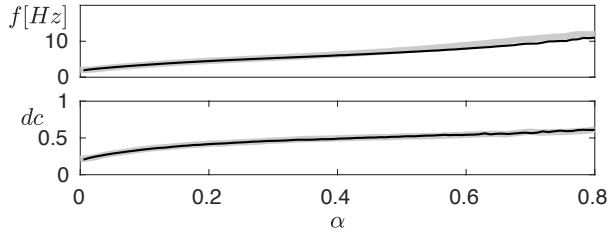

Fig. 2. Spike frequency, f, (upper panel) and duty cycle, dc, of flexor cells plotted against the parameter α in the 8-cell CPG (black curves) and in the CPG-0 circuit (gray curves, plotted underneath the black ones).

not produce the walk gait. We point out that for $\alpha < 0.14$ and for $0.78 < \alpha < 0.8$ the reduced circuit generates patterns not matching any gaits natural for quadrupeds. In particular, for $0.14 < \alpha$ there is bistability, due to a supercritical pitchfork bifurcation. The cause of such bistability can be explained by comparing the time evolution of cells 1, 2 and 5 in the 8-cell CPG and of cells 1 and 2 in the CPG-0 at low α-values, see Fig. 4. The original circuit is designed so that, whenever the active pre-synaptic cell-1 fires (produces an action potential), the outgoing inhibitory synapse projected onto the post-synaptic cell-2 is activated and thus prevents (delays) the latter from producing any action potential. When cell-1 becomes quiescent (inactive), cell-5 is active and again inhibits cell-2, which yet remains inactive in a silent state. As soon as cell-5 becomes silent, it is the turn for cell-2 to

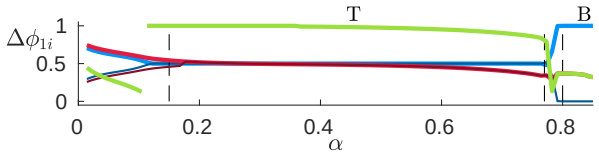

Fig. 3. Bifurcation diagram of the CPG-0 circuit. Phase lags $\Delta\phi_{1i}$ between the reference cell 1 and other cells: $i = 2$ (blue lines), $i = 3$ (red lines), $i = 4$ (green lines), plotted against increasing (dark colors) and decreasing (light colors) the parameter α reveals the presence of hysteresis (i.e., bistability).

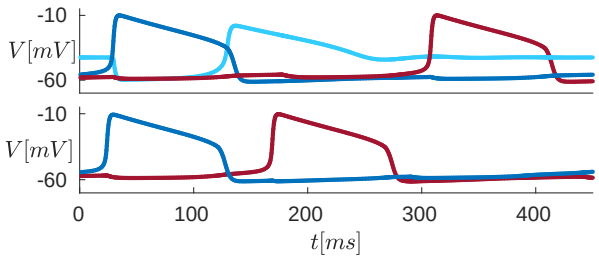

Fig. 4. Time evolution of the membrane potentials in cells 1 (blue), 2 (red) and 5 (light-blue) of the 8-cell CPG (upper panel) and in cells 1 (blue) and 2 (red) of CPG-0 (lower panel) at $\alpha = 0.01$.

generate an action potential due to the effect of post-inhibitory rebound. As the result, the circuit operates as if connections with extensor cell-5 could have provided a delayed inhibition between flexor cells 1 and 2.

Removing cell-5 in the reduced CPG-0, lets cell-2, using post-inhibitory rebound, fire right after cell-1 becomes silent and turns its inhibition off. Because of the network symmetry, cells 1 and 2 do not become phase-locked in proper anti-phase; moreover, with reversed initial conditions the roles of cells 1 and 2 are swapped, i.e., cell-1 would fire right after cell 2 becomes silent and *vice versa*. This explains bistability of patters generated by the CPG-0 circuit at low α values. With higher α values, the duty cycle increases and the inhibition from extensors to flexors is no longer necessary to ensure their anti-phase phase locking.

Based upon the above observations, below we will devise and analyze two 4-cell CPGs (CPG-A and CPG-B) with additional connections with respect to the CPG-0 circuit. Our aim is to design minimal rhythmic circuits that, in addition to trot and bound, can also generate the walk gait, like the original 8-cell CPG.

B. CPG-A circuit

This circuit (shown in Fig. 1(c)) mimics the action of each extensor cell and of its delayed inhibition to flexors by adding four inhibitory synapses with delay (orange connections in Fig. 1(c)) with the following activation function:

$$h^d_{in}(V_i, V_j) = \frac{E_{in} - V_i(t)}{1 + e^{\nu(V_j(t-\tau)-\theta)}}, \qquad (1)$$

where τ is the synapse delay, $\nu = 0.3$ [mV^{-1}], $E_{in} = -75$ [mV] and $\theta = -30$ [mV]. To evaluate the range of fitting τ-values, we compute the delay between the activation of flexor and corresponding extensor in the 8-cell CPG. The results, depicted in Fig. 5, indicate that τ must range between 80 and

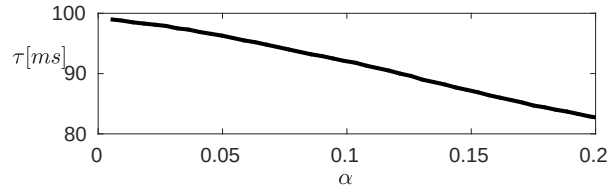

Fig. 5. Dependence of the time delay between the activation of flexor and corresponding extensor cells in the 8-cell CPG on the parameter α.

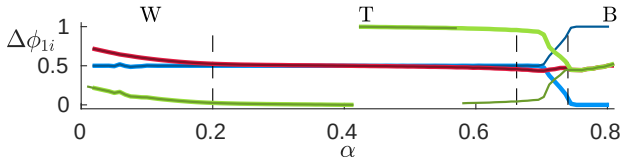

Fig. 6. Bifurcation diagram of the CPG-A circuit: forward and backward transformation of phase lags $\Delta\phi_{1i}(\alpha)$, $i = 2$ (blue lines), $i = 3$ (red lines), $i = 4$ (green lines), as the bifurcation α-parameter is increased (dark colors) and decreased (light colors) points out the absence of bistability. Stability regions of walk (W) trot (T) and bound (B) gaits are evident.

100 [ms] for low α values, so we get the mean value $\tau = 90$ [ms]. The bifurcation diagram shown in Fig. 6 displays that the reduced CPG-A circuit can produce the three desired gaits: walk, trot and bound, all observed in the 8-cell CPG. The discontinuities in the trot (T) region are just illusory, due to the phase lag definition ($\Delta\phi_{1i}(t) = (\phi_i(t) - \phi_1(t)) \mod 1$).

C. CPG-B circuit

With respect to CPG-0, this circuit (shown in Fig. 1(d)) is additionally populated with synapses between fore and hind flexors to generate all gaits. For low α values, it generates periodically a traveling-wave pattern with cells activating in the following order: 1-4-2-3. Thus, an alternative way to ensure that when cell-1 becomes silent cell-4 fires instead of cell-3 is adding to CPG-0 inhibitory synapses between cells 1-3, as shown in Fig. 1(d). The same holds for cell-2 (which plays the role of cell-1) and cells 3-4 (which swap their roles).

The bi-parametric bifurcation diagram shown in Fig. 7 lets us evaluate the synaptic strength g_c of these unidirectional connections and select the piecewise-affine (PWA) function $g_c(\alpha)$ (black line in the diagram) ensuring that cells 1 and 2 always fire in the locked anti-phase state. The PWA function is chosen so that its effect on the behavior of the CPG is minimal, while it helps to maintain the synchronization between fore and hind cells. In other words, the value of g_c is chosen as small as possible to ensure the robust phase lag $\Delta\phi_{12} = 0.5$ in the walking gait. Because for $\alpha > 0.14$ the CPG-B circuit can generate the desired gaits without a need for any new synapses, g_c is set to 0. The red line in Fig. 7 demarcates the border (supercritical pitchfork bifurcation) between two regions of monostable (yellow region) and bistable dynamics. It is determined by applying a brute-force criterion (edge of the yellow region). In the blueish-color region bounded by the red border, the circuit generates pair-wise rhythmic patterns: one with phase lag $\Delta\phi_{12}$ locked at the value shown in the vertical bar, while the other with phase lag locked at $1 - \Delta\phi_{12}$, as in Fig. 3 (low α values).

To elucidate all possible gaits produced by the CPG-B

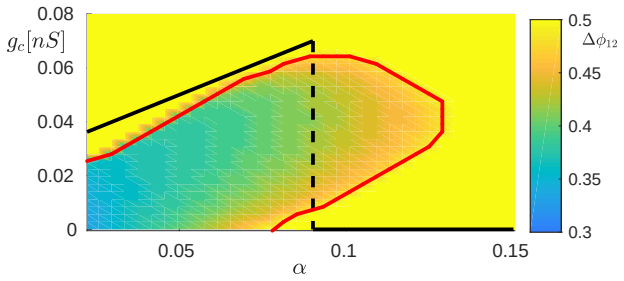

Fig. 7. Brute-force bifurcation diagram obtained by varying α and g_c in CPG B. Chosen PWA function $g_c(\alpha)$ (black line). Curve marking the edge between monostability and bistability regions (red line).

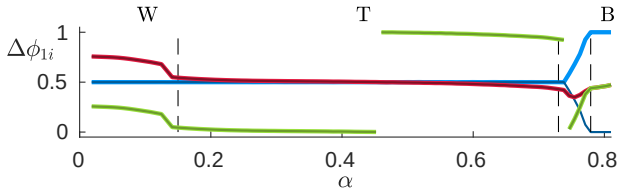

Fig. 8. Bifurcation diagram of CPG-B with synaptic strength of added synapses $g_c(\alpha)$ (see Fig. 7). $\Delta\phi_{1i}(\alpha)$, with $i = 2$ (blue lines), $i = 3$ (red lines), $i = 4$ (green lines), is obtained by increasing (dark colors) or decreasing (light colors) the bifurcation parameter α. The bifurcation diagrams point out the presence of three regions where walk (W), trot (T) and bound (B), respectively, are the only stable gaits.

circuit, we perform the bifurcation sweep of its state as the brainstem-drive α is varied and by setting the new synapses strength according to $g_c(\alpha)$. The bifurcation diagram shown in Fig. 8 confirms that the CPG-B produces all the desired gaits.

III. Neuromechanical Model

In this section we extend the previous model to make it suitable for applications in quadruped robots. We focus on CPG-B, as it has the minimum number of cells and synapses (14 vs 16 of CPG-A). There is a large number of neuromechanical models with different complexities and levels of biophysical realism [10]–[14]. Here, we consider only thigh and hip of each leg and we add to our CPG a very simple biophysically plausible model derived from [10], [13].

Each limb is modeled as a pendulum, of length L and mass m, as sketched in Fig. 9. The extensor (flexor) muscle produces a force F_E (F_F) perpendicular to the leg that can move the limb anti-clockwise (clock-wise). Then, the equation of motion

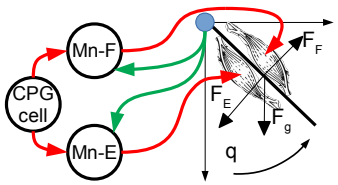

Fig. 9. Neuromechanical model of a single limb. Extensor and flexor are driven by motor-neurons Mn-E and Mn-F (red arrows). The motor-neurons are driven by the CPG cell (red arrows) and their activity is also influenced by the feedback from the mechanical model (green arrows). The forces acting on the limb are represented by black arrows.

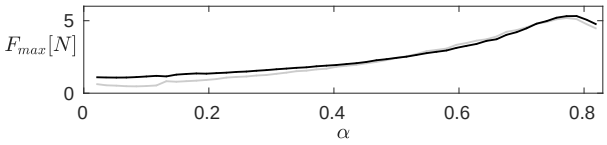

Fig. 10. The chosen functions $F_{max}(\alpha)$ for flexor (black line) and extensor (gray line) muscles.

TABLE I. PARAMETERS OF THE NEUROMECHANICAL MODEL.

L	0.3 m	q_{min}	-0.0873 rad ($-5°$)
m	300g	q_{max}	0.1396 rad ($8°$)
b	0.2 $\frac{kgm^2}{s \cdot rad}$	ν_A	5 mV^{-1}
ν_q	50 rad^{-1}	θ_A	-43 mV

of each thigh is given by:

$$I\ddot{q} = F_F \frac{L}{2} - F_E \frac{L}{2} - \underbrace{mg}_{F_g} \sin(q) - b\dot{q}, \qquad (2)$$

where q is the angle between the leg and the normal to ground, $I = \frac{mL^2}{3}$ is the momentum of inertia and b is the angular viscosity of the joint. The force of each muscle is evaluated as $F = F_{max}A$, where A is the activation of the driving motor-neuron, that is a number ranging in the interval $[0, 1]$ and related to the muscle activation level. We design a neuronal network driving the limbs subjected to three constraints: (1) each leg must be synchronized with the corresponding CPG cell when no external force is applied; (2) each leg must oscillate within the range $[q_{min}, q_{max}]$; (3) when an external force is applied and next released, the leg should be able to re-synchronize with its driving cell.

The designed network employs CPG-B to drive (with the i-th cell) the two motor-neurons, which, in turn, drive the muscles (Fig. 9). Moreover, we add two sensory feedback loops from hip to motor-neurons, whose activation properties are borrowed from [10] and described by the following equation (a completely similar equation holds for $f^{(i)}_{max}$):

$$f^{(i)}_{min} = \frac{1}{1 + e^{\nu_q (q^{(i)} - q^{(i)}_{min})}}. \qquad (3)$$

The motor-neuron activation $A^{(i)}$ for the i-th leg is computed as an algebraic function of the CPG cell membrane potential V_i and the feedback from the hip (Eq. (3)) as follows (blue: flexor, red: extensor, black: both):

$$\begin{matrix} A^{(i)}_F \\ A^{(i)}_E \end{matrix} = max \left(\frac{1}{1 + e^{-\nu_A (V_i - \theta_V)}} - 2 \begin{matrix} f^{(i)}_{max} \\ f^{(i)}_{min} \end{matrix}, 0 \right), \qquad (4)$$

where all parameter values are listed in Tab. I; in particular, the mechanical parameters are chosen to be identical to those of the Oncilla robot [10]. Here, function F_{max} of α is chosen on the basis of extensive simulations with CEPAGE, thus ensuring that $q^{(i)}$ varies between q_{max} and q_{min} (see Fig. 10).

The fulfillment of constraint (1) follows from the bifurcation diagram, shown in Fig. 11, obtained in the absence of any external force. It demonstrates that the legs synchronize with the driving cells, as we expect. Figure 12 shows the maximum and minimum angles for different values of α; it is evident that the constraint (2) on angle range ($[-5°, 8°]$) is satisfied.

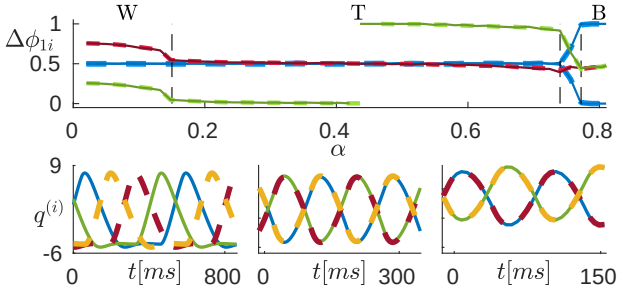

Fig. 11. Upper panel: bifurcation diagram of the neuromechanical model showing the locked phase lags $\Delta\phi_{1i}(\alpha)$, with $i = 2$ (blue lines), $i = 3$ (red lines), $i = 4$ (green lines), between CPG-B cells' membrane potentials (solid lines) or limbs' angles (dashed lines) in the absence of external force. The diagram evidences again three stability regions corresponding to walk (W), trot (T) and bound (B) gaits. Lower panels: angles $q^{(i)}(t)$ for the four legs (color code as for the corresponding cells in Fig. 1(d)).

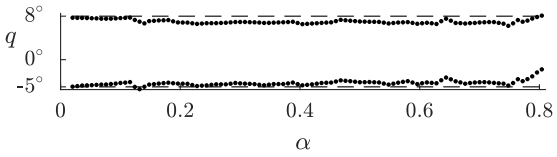

Fig. 12. Maximal and minimal values (black dots) for the angle q for different α values. Dashed lines represent constraints imposed on q.

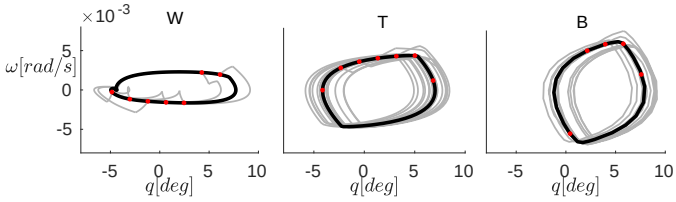

Fig. 13. Stable periodic orbits (black lines) and perturbed trajectories (gray lines) of a single leg for walk (W), trot (T) and bound (B). The red dots mark the perturbations applied.

To measure the robustness of the whole system, we perturb a targeted limb with an external force of about $0.1N$ for 0.1 seconds at various limb angles and speeds in case of all three gaits generated by the CPG circuit. One can see from the phase-space panels in Fig. 13 that as soon as the external force is removed, every leg quickly re-synchronizes with the corresponding CPG cell in all three cases examined.

IV. CONCLUSIONS

The modeling of CPGs requires a trade-off between two conflicting interests: *simplicity* of the circuit for its analysis and implementation against its *fidelity to biophysics* to reproduce the original gaits not only qualitatively but also quantitatively in practical applications. This paper presents another step forward in this direction: the technique proposed in [4], with the use of the Ockham's razor, let us stably re-create some desired gaits in two simplified CPG circuits. Furthermore, the addition of a neuromechanical model brings the synthetically developed CPGs taking into account local feedback loops even closer to engineering robotic applications [10].

Acknowledgments: Work supported by University of Genoa, by NSF (grant IOS-1455527) and by Lobachevsky University of Nižnij Novgorod (grant 14-41-00044).

REFERENCES

[1] A. J. Ijspeert, "Central pattern generators for locomotion control in animals and robots: a review," *Neural Networks*, vol. 21, no. 4, pp. 642–653, 2008.

[2] A. Kozlov, M. Huss, A. Lansner, J. H. Kotaleski, and S. Grillner, "Simple cellular and network control principles govern complex patterns of motor behavior," *Proceedings of the National Academy of Sciences*, vol. 106, no. 47, pp. 20 027–20 032, 2009.

[3] Y. I. Molkov, B. J. Bacak, A. E. Talpalar, and I. A. Rybak, "Mechanisms of left-right coordination in mammalian locomotor pattern generation circuits: A mathematical modeling view," *PLoS Computational Biology*, vol. 11, no. 5, pp. 1–40, 2015.

[4] M. Lodi, A. L. Shilnikov, and M. Storace, "Design of synthetic central pattern generators producing desired quadruped gaits," *IEEE Transactions on Circuits and Systems I: Regular papers*, 2017, in the press, doi: 10.1109/TCSI.2017.2759320.

[5] M. Lodi, A. Shilnikov, and M. Storace, "CEPAGE: A toolbox for Central Pattern Generator analysis," in *Proc. of 2017 IEEE International Symposium on Circuits and Systems (ISCAS)*, Baltimore, MD, USA, May 28–31, 2017, pp. 1266–1269.

[6] S. M. Danner, S. D. Wilshin, N. A. Shevtsova, and I. A. Rybak, "Central control of interlimb coordination and speed-dependent gait expression in quadrupeds," *The Journal of Physiology*, vol. 594, no. 23, pp. 6947–6967, 2016.

[7] J. Wojcik, J. Schwabedal, R. Clewley, and A. L. Shilnikov, "Key bifurcations of bursting polyrhythms in 3-cell central pattern generators," *PLOS One*, vol. 9, no. 4, p. e92918, 2014.

[8] J. Schwabedal, A. Neiman, and A. L. Shilnikov, "Robust design of polyrhythmic neural circuits," *Physics Review E*, vol. 90, no. 2, p. 022715, 2014.

[9] J. Schwabedal, D. Knapper, and A. L. Shilnikov, "Qualitative and quantitative stability analysis of penta-rhythmic circuits," *Nonlinearity*, vol. 29, no. 12, pp. 3647–3676, 2016.

[10] C. Ferreira and C. P. Santos, "A sensory-driven controller for quadruped locomotion," *Biological cybernetics*, vol. 111, no. 1, pp. 49–67, 2017.

[11] S. N. Markin, A. N. Klishko, N. A. Shevtsova, M. A. Lemay, B. I. Prilutsky, and I. A. Rybak, "Afferent control of locomotor CPG: insights from a simple neuromechanical model," *Annals of the New York Academy of Sciences*, vol. 1198, no. 1, pp. 21–34, 2010.

[12] N. S. Szczecinski, A. J. Hunt, and R. D. Quinn, "Design process and tools for dynamic neuromechanical models and robot controllers," *Biological cybernetics*, vol. 111, no. 1, pp. 105–127, 2017.

[13] F. Dzeladini, J. Van Den Kieboom, and A. Ijspeert, "The contribution of a central pattern generator in a reflex-based neuromuscular model," *Frontiers in Human Neuroscience*, vol. 8, pp. 371 (1–18), 2014.

[14] L. E. Spardy, S. N. Markin, N. A. Shevtsova, B. I. Prilutsky, I. A. Rybak, and J. E. Rubin, "A dynamical systems analysis of afferent control in a neuromechanical model of locomotion: II. Phase asymmetry," *Journal of Neural Engineering*, vol. 8, no. 6, pp. 065 004 (1–19), 2011.